

# Collective excitations and universal coarsening dynamics of a spin-orbit-coupled spin-1 Bose-Einstein condensate

Rajat,<sup>1,\*</sup> Paramjeet Banger,<sup>1,2,†</sup> and Sandeep Gautam<sup>1,‡</sup>

<sup>1</sup>*Department of Physics, Indian Institute of Technology Ropar, Rupnagar 140001, Punjab, India*

<sup>2</sup>*Department of Physics, Indian Institute of Science Education and Research Pune, Pune 411008, India*

We study the collective excitation spectrum of a Raman-induced spin-orbit-coupled spin-1 Bose-Einstein condensate confined in a quasi-one-dimensional harmonic trap while varying either the Raman coupling or quadratic Zeeman field strength by using the Bogoliubov approach. A few low-lying modes, which can be used to delineate the phase boundaries, are identified by exciting them with suitable perturbations. We also investigate the coarsening dynamics of a homogeneous quasi-two-dimensional spin-orbit-coupled spin-1 condensate by quenching from the zero-momentum into the plane wave phase through a sudden change in Raman coupling or quadratic Zeeman field strength. We demonstrate that the correlation function of the order parameter displays dynamic scaling during the late-time dynamics, allowing us to determine the dynamic critical exponent.

## I. INTRODUCTION

One of the remarkable accomplishments in ultracold quantum gases is the creation of artificial gauge potentials, which allows neutral ultracold atoms to mimic the behavior of charged particles in external electric or magnetic fields [1, 2]. Synthetic gauge fields can be designed to interact with internal degrees of freedom, like atomic spin. This process involves coupling each atom's spin with its center-of-mass motion, commonly known as spin-orbit (SO) coupling. [2, 3]. Experimental realizations of spin-orbit coupling in ultracold neutral atomic gases [4–6] has provided a novel route to study exotic quantum phases and nonlinear dynamics [7].

In a Raman-induced SO-coupled Bose-Einstein condensate (BEC), various ground state phases can emerge, including the supersolid stripe (ST) phase, the plane wave (PW) phase, and the zero momentum (ZM) phase [8–10]. The ST phase has been identified as having supersolid properties as it spontaneously breaks both the gauge and continuous translational symmetry [11–13]. The PW phase breaks  $\mathbb{Z}_2$  symmetry and features non-zero magnetization [9, 14, 15]. The PW and the ST phases correspond to condensation in a single and a pair of plane-wave states, respectively, while in the ZM phase, BEC occurs in the zero-momentum state [9]. Since the achievement of BEC, investigating collective excitations has become an essential tool for gaining insight into the macroscopic quantum phenomena that govern these systems [16, 17]. In the SO-coupled pseudo-spinor BECs, the excitation spectrum can demarcate the phase boundaries in both uniform [18–21] and harmonically trapped systems [13, 22–24]. It has now been established that as the Raman coupling strength decreases, the roton gap in the dispersion of the PW phase also decreases and eventually closes at the boundary between the PW and ST phases [20–22, 25].

The excitation spectrum of the homogeneous SO-coupled spin-1 BECs, which can feature a double roton-maxon structure, has also been used to discern the phase boundaries be-

tween different phases [15, 26, 27]. Additionally, it has been observed that at small values of Raman coupling ( $\Omega$ ) and quadratic Zeeman field strength ( $\epsilon$ ), a direct transition from the ZM to the ST phase can occur characterized by symmetric double rotons [15, 26], which are unique to spin-1 BECs. As the transition point approaches, the double rotons soften, indicating the system's tendency toward crystallization. The collective excitations of a trapped quasi-one-dimensional (quasi-1D) spin-1 BEC with spin coupling the linear momentum but crucially, without Raman coupling and quadratic Zeeman field strength have been studied at zero and finite temperatures [28]. Due to the absence of Raman coupling and quadratic Zeeman field strength, typical features of Raman-induced SO-coupled, like supersolid phase, roton-maxon structure, etc., do not emerge in such a system. Besides the theoretical studies on the homogeneous SO-coupled spin-1 BECs, the collective excitation spectrum of a trapped Raman-induced SO-coupled spin-1 BEC [5, 6] remains uninvestigated. This gap in the literature motivates us to study the collective excitation spectrum of a harmonically confined Raman-induced SO-coupled BEC.

Collective modes play an important role in the sudden quench dynamics [29, 30], where the excitation spectra of the post-quench initial states highlight dynamically unstable modes [29]. It is essential to account for fluctuations beyond the mean-field order to encourage the growth of unstable modes triggered by the sudden change. The truncated Wigner prescription provides an effective way to introduce fluctuations into the initial state [31]. When a system undergoes a quench from a disordered to an ordered phase, the growth of order occurs through the formation of phase domains [32]. The size of these domains is generally governed by a characteristic length scale,  $L(t)$ , which increases as the system evolves. Once this length scale surpasses certain microscopic thresholds, the phase ordering process often becomes universal, following a power-law growth  $L(t) \sim t^\beta$ , where  $\beta$  is dynamic critical exponent. Universal coarsening dynamics, which describe this growth, have been theoretically studied in binary [33–35] and spin-1 spinor BECs [29, 36–48], particularly in quasi-1D [47, 49] and quasi-two-dimensional (quasi-2D) configurations for quenching into both easy-axis and easy-plane ferromagnetic phases [42, 46]. Experimental

\* rajat.19phz0009@iitrr.ac.in

† paramjeet.banger@acads.iiserpune.ac.in

‡ sandeep@iitrr.ac.in

studies have also confirmed the universal relaxation dynamics in spinor [30, 50, 51] and isolated Bose gases [52–54]. However, the universal coarsening dynamics of an SO-coupled spinor BEC with a qualitatively distinct phase diagram have not been studied.

In the first part of this study, we theoretically investigate the collective excitations of a harmonically trapped quasi-1D Raman-induced SO-coupled spin-1 BEC as a function of coupling and quadratic Zeeman field strengths. In the second part, we study the ensuing dynamics in a homogenous quasi-2D SO-coupled spin-1 BEC in the (non-magnetized) ZM phase after a sudden quench of Raman coupling or quadratic Zeeman field strength to a value corresponding to which the ground state phase is the (magnetized) PW phase. We demonstrate that over the extended timescales following the quench, a universal scaling regime emerges, wherein the order-parameter autocorrelation functions at different times collapse onto a universal scaling function (independent of time) when the spatial variable is rescaled by a characteristic length  $L(t)$ , which shows a power law increase with time.

The paper is organized as follows. In Sec. II, we introduce the mean-field model to study a Raman-induced SO-coupled spin-1 BEC. In Sec. II A, we present the Bogoliubov-de Gennes (BdG) equations for the system. In Sec. II B, we discuss the methodology to excite a few low-lying excitations via suitable perturbations to the Hamiltonian. Sec. III discusses the phase diagram and the collective excitation spectrum of a harmonically confined quasi-1D SO-coupled BEC. We then turn our attention to the universal coarsening dynamics of a homogeneous quasi-2D SO-coupled spin-1 BEC in Sec. IV, focusing on the sudden quench of Raman coupling, which triggers phase transition from the ZM phase to the PW phase. Finally, in Sec. V, we conclude with a summary of the key findings of this study.

## II. MODEL

The ground state properties of an SO-coupled spin-1 BEC can be analyzed by minimizing the energy functional [5, 6, 14, 55]

$$E[\Phi] = \int d\mathbf{r} \left\{ \Phi^\dagger H_0 \Phi + \frac{c_0}{2} (\Phi^\dagger \Phi)^2 + \frac{c_2}{2} (\Phi^\dagger \mathbf{f} \Phi)^2 \right\}, \quad (1)$$

where  $m$  is the atomic mass,

$$H_0 = \frac{\hbar^2}{2m} \left( -\iota \frac{\partial}{\partial x} + 2k_R f_z \right)^2 - \frac{\hbar^2}{2m} \left( \frac{\partial^2}{\partial y^2} + \frac{\partial^2}{\partial z^2} \right) + V(\mathbf{r}) + \Omega f_x + \epsilon f_z^2, \quad (2)$$

is the single-particle Hamiltonian,  $\Phi$  is the three-component condensate wave function with  $\int |\Phi|^2 d\mathbf{r}$  equal to the number of atoms  $N$ ,  $V(\mathbf{r})$  is the harmonic oscillator potential,  $\mathbf{f} = (f_x, f_y, f_z)$  is a vector of spin-1 matrices,  $c_0 = 4\pi\hbar^2(a_0 + 2a_2)/3m$  and  $c_2 = 4\pi\hbar^2(a_2 - a_0)/3m$  stand for spin-independent and spin-dependent interactions, written in terms of the  $s$ -wave scattering lengths  $a_0$  and  $a_2$  of binary col-

lisions with total spin equal to 0 and 2, respectively. In Eq. (2),  $\Omega$  and  $k_R$  are the Raman and spin-orbit coupling strengths, respectively, and  $\epsilon$  is the quadratic Zeeman field strength [5]. Depending on the sign of  $c_2$ , a spin-1 BEC can have ferromagnetic ( $c_2 < 0$ ) or antiferromagnetic ( $c_2 > 0$ ) interactions, and in this manuscript, we consider a spin-1 BEC with antiferromagnetic interactions. To study the dynamics of the system, it is convenient to introduce the Lagrangian

$$L = \int d\mathbf{r} \frac{i\hbar}{2} \left( \Phi^\dagger \frac{\partial \Phi}{\partial t} - \Phi \frac{\partial \Phi^\dagger}{\partial t} \right) - E[\Phi]. \quad (3)$$

In the first part of this manuscript, we consider a quasi-1D SO-coupled spin-1 BEC of  $^{23}\text{Na}$  in a highly anisotropic axially symmetric harmonic trap with significantly stronger confinement along the radial than the axial direction. The action principle leads to the coupled Gross-Pitaevskii equations (GPEs), which in the dimensionless form are [5, 6, 56]

$$\begin{aligned} \iota \frac{\partial \phi_{\pm 1}}{\partial t} = & \left[ -\frac{1}{2} \partial_x^2 + 2k_R^2 \mp \iota 2k_R \partial_x + V(x) + \epsilon + c_0 n \right] \phi_{\pm 1} \\ & + c_2 (n_{\pm 1} + n_0 - n_{\mp 1}) \phi_{\pm 1} + c_2 \phi_0^2 \phi_{\mp 1}^* + \frac{\Omega}{\sqrt{2}} \phi_0, \end{aligned} \quad (4a)$$

$$\begin{aligned} \iota \frac{\partial \phi_0}{\partial t} = & \left[ -\frac{1}{2} \partial_x^2 + V(x) + c_0 n + c_2 (n_{+1} + n_{-1}) \right] \phi_0 \\ & + 2c_2 \phi_{+1} \phi_0^* \phi_{-1} + \frac{\Omega}{\sqrt{2}} (\phi_{+1} + \phi_{-1}), \end{aligned} \quad (4b)$$

where  $V(x) = x^2/2$  is the harmonic trapping potential along the axial  $x$ -direction,  $n_j = |\phi_j(x)|^2$  and  $n = \sum_j n_j$  are the component and total densities, respectively, with  $\int n(x) dx = 1$ . In Eqs. (4a) and (4b) time, length, and energy are in the units of  $\omega_x^{-1}$ ,  $l_0 = \sqrt{\hbar/m\omega_x}$ , and  $\hbar\omega_x$ , respectively, where  $\omega_x$  is the trap frequency along the weakly confined axial direction. The dimensionless interaction strengths are  $c_0 = 2(a_0 + 2a_2)\kappa/(3l_0)$  and  $c_2 = 2(a_2 - a_0)\kappa/(3l_0)$  with  $\kappa$  as the ratio of the trap frequencies along the radial direction to the axial direction. For the stationary solutions, substituting  $\phi_j(x, t) = \phi_j(x)e^{-\iota\mu t}$ , where  $\mu$  denotes the chemical potential, in Eqs. (4a)-(4b) yields the time-independent version of the GPEs. To investigate the collective excitation spectrum of the quasi-1D SO-coupled BEC, first, we use the Bogoliubov-de Gennes (BdG) equations and then validate our results by exciting a few collective modes with suitable perturbations to the Hamiltonian.

### A. Bogoliubov-de Gennes (BdG) equations

We employ the Bogoliubov approach to investigate the collective excitation spectrum. Here, one incorporates the fluctuations to the ground state leading to the perturbed order parameter

$$\phi_j(x, t) = e^{-\iota\mu t} [\phi_j(x) + \delta\phi_j(x, t)], \quad (5)$$

where  $\phi_j(x)$  is the  $j$ th component's ground-state wavefunction,  $\delta\phi_j(x, t) = u_j^\lambda(x)e^{-i\omega_\lambda t} - v_j^{\lambda*}(x)e^{i\omega_\lambda t}$  with  $u_j^\lambda(x)$  and  $v_j^\lambda(x)$  denoting the Bogoliubov amplitudes and  $\omega_\lambda$  the excitation frequency. The GPEs (4a) and (4b) are linearized to obtain BdG equations,

$$\begin{pmatrix} \mathcal{A} & -\mathcal{B} \\ \mathcal{B}^* & -\mathcal{A}^* \end{pmatrix} \begin{pmatrix} \mathbf{u}^\lambda \\ \mathbf{v}^\lambda \end{pmatrix} = \omega_\lambda \begin{pmatrix} \mathbf{u}^\lambda \\ \mathbf{v}^\lambda \end{pmatrix}, \quad (6)$$

where  $\mathbf{u}^\lambda = (u_{+1}^\lambda, u_0^\lambda, u_{-1}^\lambda)^T$ ,  $\mathbf{v}^\lambda = (v_{+1}^\lambda, v_0^\lambda, v_{-1}^\lambda)^T$ ,  $\mathcal{A}$  and  $\mathcal{B}$  are  $3 \times 3$  matrices, and  $*$  denotes the complex conjugate. The elements of the  $\mathcal{A}$  and  $\mathcal{B}$  are defined as follows:

$$\begin{aligned} \mathcal{A}_{11} &= \left( -\frac{1}{2}\partial_x^2 - \mu + \epsilon + 2k_R^2 + V(x) + c_0 n \right) \\ &\quad + c_0 n_{+1} + c_2(2n_{+1} + n_0 - n_{-1}) - i2k_R \partial_x, \\ \mathcal{A}_{12} &= (c_0 + c_2)(\phi_0^* \phi_{+1}) + 2c_2(\phi_{-1}^* \phi_0) + \frac{\Omega}{\sqrt{2}}, \\ \mathcal{A}_{13} &= (c_0 - c_2)(\phi_{-1}^* \phi_{+1}), \\ \mathcal{A}_{22} &= \left( -\frac{1}{2}\partial_x^2 - \mu + V(x) + c_0 n \right) \\ &\quad + c_0 n_0 + c_2(n_{+1} + n_{-1}), \\ \mathcal{A}_{23} &= (c_0 + c_2)(\phi_0 \phi_{-1}^*) + 2c_2(\phi_{+1} \phi_0^*) + \frac{\Omega}{\sqrt{2}}, \\ \mathcal{A}_{33} &= \left( -\frac{1}{2}\partial_x^2 - \mu + \epsilon + 2k_R^2 + V(x) + c_0 n \right) \\ &\quad + c_0 n_{-1} + c_2(2n_{-1} + n_0 - n_{+1}) + i2k_R \partial_x, \\ \mathcal{A}_{21} &= \mathcal{A}_{12}^*, \quad \mathcal{A}_{31} = \mathcal{A}_{13}^*, \quad \mathcal{A}_{32} = \mathcal{A}_{23}^*, \\ \mathcal{B}_{11} &= (c_0 + c_2)\phi_{+1}^2, \quad \mathcal{B}_{12} = (c_0 + c_2)\phi_0 \phi_{+1} + \frac{\Omega}{\sqrt{2}}, \\ \mathcal{B}_{13} &= (c_0 - c_2)\phi_{-1} \phi_{+1} + c_2 \phi_0^2, \quad \mathcal{B}_{22} = c_0 \phi_0^2 + 2c_2 \phi_{+1} \phi_{-1}, \\ \mathcal{B}_{23} &= (c_0 - c_2)\phi_{+1} \phi_{-1} + c_2 \phi_0^2 + \frac{\Omega}{\sqrt{2}}, \quad \mathcal{B}_{33} = (c_0 + c_2)\phi_{-1}^2, \\ \mathcal{B}_{21} &= \mathcal{B}_{12}, \quad \mathcal{B}_{31} = \mathcal{B}_{13}, \quad \mathcal{B}_{32} = \mathcal{B}_{23}. \end{aligned}$$

We solve one-dimensional GPEs (4a) and (4b) numerically using a split time-step Fourier pseudospectral method and calculate the ground-state solution using imaginary-time propagation [57]. We consider a spatial step size  $\Delta x = 0.01$  and an imaginary-time step of  $10^{-5}$  in the imaginary-time propagation. We solve the BdG equations for a harmonically confined BEC by expanding the quasiparticle amplitudes in terms of the eigenfunctions of the one-dimensional harmonic oscillator, which leads to a generalized matrix eigenvalue problem for the expansion coefficients [58]. We then solve this eigenvalue problem using standard conventional matrix diagonalization subroutines [59, 60] to obtain the eigenenergies ( $\omega_\lambda$ ) and quasiparticle amplitudes ( $u^\lambda$  and  $v^\lambda$ ). In this work, we consider a truncated basis set of 180 low-lying harmonic oscillator eigenstates to expand quasiparticle amplitudes. We have confirmed that increasing the basis size does not affect the results for low-lying collective excitations of the quasi-1D

system considered in this work.

### B. Time-dependent Gross-Pitaevskii equation with perturbations

A few low-lying collective excitations of a spinor BEC, like dipole, spin-dipole, breathing, and spin-breathing modes, can be excited by perturbing the underlying Hamiltonian with a suitable perturbation [61, 62]. These modes are of great interest and can be investigated in experiments. Conceptually, to excite these modes, one can perturb the trapping potential as follows:

$$V(x) = \begin{cases} \frac{1}{2} \left( x + \delta \times \hat{O} \right)^2 & \text{for dipole modes} \\ \frac{1}{2} \left( x^2 + \delta \times \hat{O} \right) & \text{for breathing modes} \end{cases}. \quad (7)$$

where  $\hat{O}$  is an observable and  $\delta$  is a small real number. Depending on the mode to be excited, the observable  $\hat{O}$  is of form

$$\hat{O} = \begin{cases} x & \text{for the dipole mode} \\ x f_z & \text{for the spin-dipole mode} \\ x^2 & \text{for the breathing mode} \\ x^2 f_z & \text{for the spin-breathing mode} \end{cases}. \quad (8)$$

We first calculate the ground-state solution of the quasi-1D SO-coupled BEC under spin-independent harmonic confinement  $V(x) = x^2/2$  and consider this as the solution of GPEs (4a) and (4b) at  $t = 0$ . For  $t > 0$ , we suddenly switch to potential  $V(x)$  in Eq. (7) and examine  $\langle \hat{O} \rangle = \int \Phi^\dagger(x, t) \hat{O} \Phi(x, t) dx$  as a function of time and extract the collective excitation frequency from its Fourier transform.

### III. GROUND STATE PHASES AND COLLECTIVE EXCITATIONS

The general ground state solution of a quasi-1D Raman-induced SO-coupled spin-1 BEC is of the form [14]

$$\Phi(x) = \sqrt{n_0(x)} \sum_{l \in \mathbb{Z}} C_l \zeta_l e^{i l k x}, \quad (9)$$

where  $n_0(x)$  is the total density in the absence of SO-coupling,  $k$  is the condensate's momentum,  $\zeta_l$  are three-component normalized spinor, and complex coefficients  $C_l$  satisfy  $\sum_l |C_l|^2 = 1$ . In this section, we consider an SO-coupled spin-1 BEC of  $^{23}\text{Na}$  atoms with  $a_0 = 48.91 a_B$  and  $a_2 = 54.54 a_B$  [63], where  $a_B$  is the Bohr radius, and SO-coupling strength  $k_R = 3$ . The BEC is confined in a quasi-1D trap with the trapping frequencies  $\omega_x = 2\pi \times 5$  Hz and  $\kappa = 20$ . The (dimensionless) interaction strengths translate to  $c_0 = 59.44$  and  $c_2 = 2.12$  for the number of atoms  $N = 5000$ . We first consider quadratic Zeeman field strength  $\epsilon = -3E_R$ , where  $E_R = k_R^2/2$  is the recoil energy, and vary Raman coupling strength  $\Omega$ . As  $\Omega$  is progressively increased,

the system first undergoes a phase transition from the ST to the PW phase above a critical coupling  $\Omega_{c_1} \approx 3.4E_R$  and then a phase transition from the PW to the ZM phase above a critical coupling  $\Omega_{c_2} \approx 6.9E_R$ . In Figs. 1(a)-(c), we show momentum  $k$ , components of spin-expectation per particle  $f_\nu = \int F_\nu dx$  with  $\nu = x, y, z$ , and  $f = \sqrt{f_x^2 + f_y^2 + f_z^2}$  as a function of Raman coupling strength  $\Omega$ , where  $F_\nu = \Phi(x)^\dagger f_\nu \Phi(x)$  is the  $\nu$  component of the spin-density vector with order parameter  $\Phi = (\phi_{+1}, \phi_0, \phi_{-1})^T$ . Across the ST-PW transition

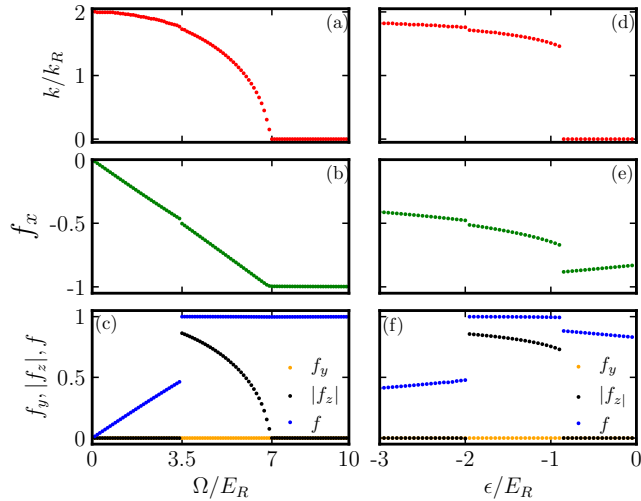


FIG. 1. The condensate's momentum and spin-expectation per particle in the ground-state phase for  $c_0 = 59.44$ ,  $c_2 = 2.12$ , and  $k_R = 3$ : (a)-(c) as a function of  $\Omega$  for a fixed  $\epsilon = -3E_R$  and (d)-(f) as a function of  $\epsilon$  for a fixed  $\Omega = 3E_R$ . (a) and (d) momentum  $k$ , (b) and (e)  $f_x = \int F_x dx$ , and (c) and (f)  $f_y = \int F_y dy$ ,  $|f_z| = |\int F_z dz|$  and  $f$  as a function of  $\Omega$ . In (a)-(c),  $k$ ,  $f_x$ ,  $|f_z|$ , and  $f$  are discontinuous at the ST-PW phase boundary  $\Omega_{c_1}$  but are continuous at the PW-ZM phase boundary  $\Omega_{c_2}$ , which illustrates the first-order and second-order natures of these two transitions, respectively. In (d)-(f), across both the critical points, the quantities change discontinuously.

point,  $k$ ,  $f_x$ ,  $|f_z|$ , and  $f$  change discontinuously. The condensate's momentum  $k$  is non-zero in the ST and PW phases only [see Fig. 1(a)];  $|f_x|$  increases linearly with an increase in  $\Omega$  in the ST and in the PW phase, while it remains constant in the ZM phase [see Fig. 1(b)];  $|f_z|$  is non-zero only in the PW phase and  $f_y$  is zero across all the three phases [see Fig. 1(c)]; and  $f$  increases linearly with  $\Omega$  in the ST phase, jumps to 1 in the PW phase, and then remains equal to 1 across the PW and the ZM phases [see Fig. 1(c)]. The variation of condensate's momentum and spin expectation per particle as a function of  $\Omega$  is qualitatively identical to the observations made for a homogeneous SO-coupled pseudospinor BEC [9]. If, rather, we fix  $\Omega = 3E_R$ , momentum  $k$  and spin-expectation per particle as a function of  $\epsilon$  are shown in Figs. 1(d), (e), and (f), respectively. In this case, too, the system first transitions from the ST to the PW above  $\epsilon_{c_1}$  and then from the PW to the ZM phase above  $\epsilon_{c_2}$ , albeit with a first-order transition across both transition points [as demonstrated by discontinuities in Figs. 1(d)-(f)].

In Fig. 2, we plot the density and the spin-density profiles for the three phases, namely the ST phase at  $\Omega = 2.5E_R$ , the PW phase at  $\Omega = 5E_R$ , and the ZM phase at  $\Omega = 7.5E_R$  for a fixed  $\epsilon = -3E_R$ . The component and the total densities oscillate in phase across the spatial extent of the BEC for the ST phase in Fig. 2(a), which is typical for a supersolid. The densities  $n_{+1}(x)$  and  $n_{-1}(x)$  overlap resulting in

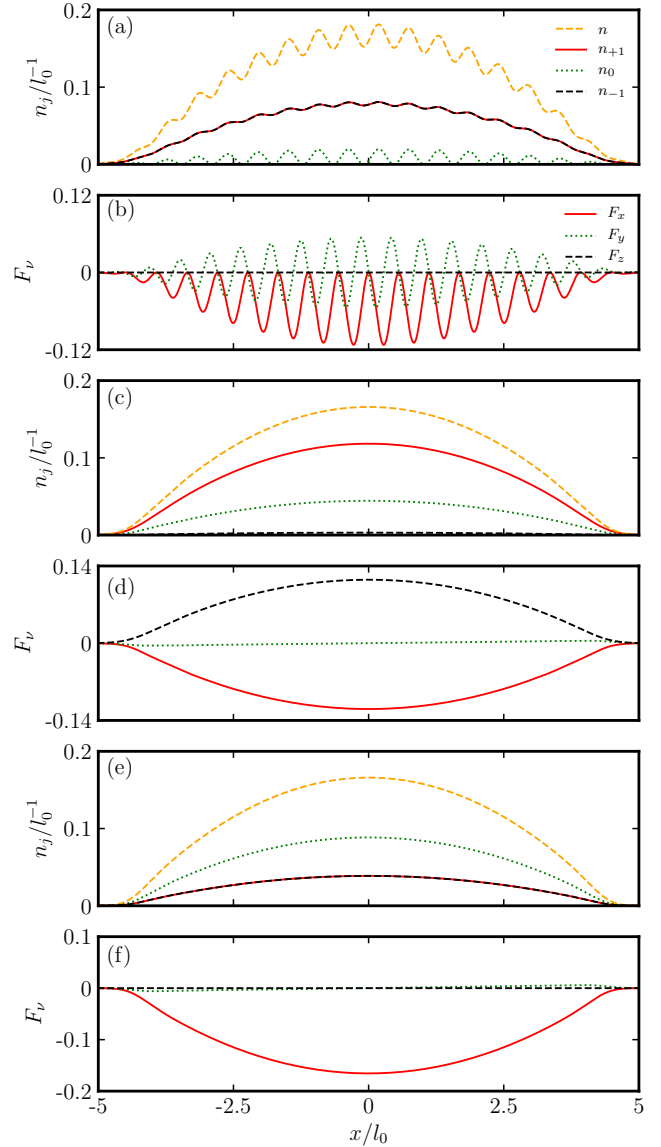


FIG. 2. Ground-state density and spin-density profiles of the SO-coupled spin-1 BEC with  $c_0 = 59.44$ ,  $c_2 = 2.12$ ,  $k_R = 3$ , and  $\epsilon = -3E_R$  in the three phases. (a) and (b) display the density and spin-density profiles in the ST phase for  $\Omega = 2.5E_R$ , (c) and (d) show the same in the PW phase for  $\Omega = 5E_R$ , and (e) and (f) illustrate the respective densities in the ZM phase for  $\Omega = 7.5E_R$ .

$F_z = 0$ , and  $F_x$  and  $F_y$  oscillate with the same period as that for densities in this phase [see Fig. 2(b)]. The PW phase with non-overlapping component densities exhibits non-zero  $F_x$  and  $F_z$  [cf. Figs. 2(c) and 2(d)]. The ZM phase again with

overlapping  $n_{+1}(x)$  and  $n_{-1}(x)$  has  $F_z = 0$ , whereas  $F_x \neq 0$  contributes to yield  $f = 1$  for this phase [see Figs. 2(e) and 2(f)].

*Collective excitations:* The phase transition in the SO-coupled spin-1 BEC can be driven varying coupling strength  $\Omega$  or quadratic Zeeman field strength  $\epsilon$  [14]. We calculate the excitation spectrum of the quasi-1D BEC as a function of these control parameters by solving the BdG Eqs. (6) as discussed in Sec. II A and confirming the nature and the magnitude of a few low-lying excitations as discussed in Sec. II B. In Fig. 3, we show the excitation spectrum of the quasi-1D SO-coupled BEC as a function of coupling strength  $\Omega$  while the  $c_0$ ,  $c_2$ ,  $k_R$ , and  $\epsilon$  are the same as in Figs. 1(a)-(c) With an

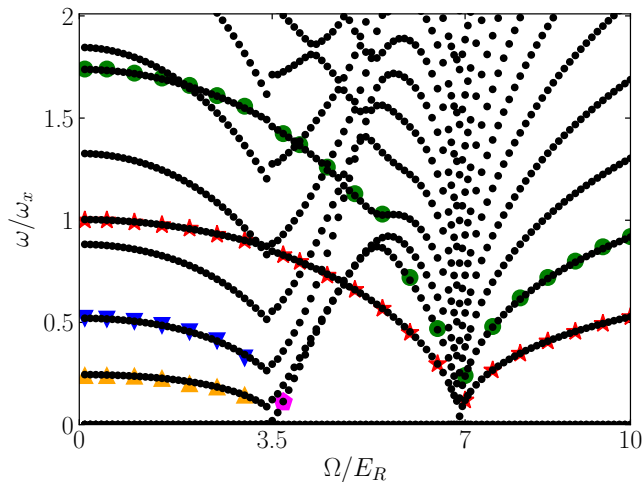


FIG. 3. Low-lying collective excitations of  $^{23}\text{Na}$  Raman-induced SO-coupled spin-1 BEC with  $c_0 = 59.44$ ,  $c_2 = 2.12$ ,  $k_R = 3$ , and  $\epsilon = -3E_R$  as a function of  $\Omega$ . The density-dipole and density-breathing modes are marked by red asterisks and green-filled circles, respectively. The yellow up-triangles and blue down-triangles indicate the spin-dipole and spin-breathing modes, respectively. At  $\Omega_{c_1} \approx 3.4E_R$ , there is a phase transition from the ST to the PW phase. Several avoided crossings, including the one involving the breathing mode, are evident in the PW phase. The density dipole mode approaches zero at  $\Omega_{c_2} \approx 6.9E_R$  above which the PW phase transitions to the ZM phase. In the PW phase, the roton excitation vanishing at the PW-ST phase boundary is marked by a magenta-coloured filled pentagon.

increase in  $\Omega$ , the low-lying collective excitations like spin-dipole, spin-breathing, density-dipole, and density-breathing modes, decrease in the ST phase. The spin-dipole and spin-breathing modes (two of the lowest non-zero energy collective excitations) have minimum energies at  $\Omega_{c_1} \approx 3.4E_R$ . The dipole and the breathing modes' excitation frequencies display discontinuities at the ST-PW phase boundary. Within the PW phase, these two modes continue to decrease with an increase in  $\Omega$  and acquire their minimum values at the PW-ZM phase boundary,  $\Omega_{c_2} \approx 6.9E_R$ . In the ZM phase, the two density modes increase with an increase in  $\Omega$ . The ST phase has two zero-energy Goldstone modes corresponding to the breaking of continuous  $U(1)$  gauge and translational symmetries. In contrast, the PW and ZM phases have one Goldstone

mode due to the breaking of  $U(1)$  gauge symmetry.

To study the collective excitations as a function of the quadratic Zeeman field strength next, we fix the Raman coupling strength at  $\Omega = 3E_R$  and vary the quadratic Zeeman strength  $\epsilon$ . The excitation spectrum as a function of  $\epsilon$  is shown in Fig. 4. Similar to the results shown in Fig. 3, within the

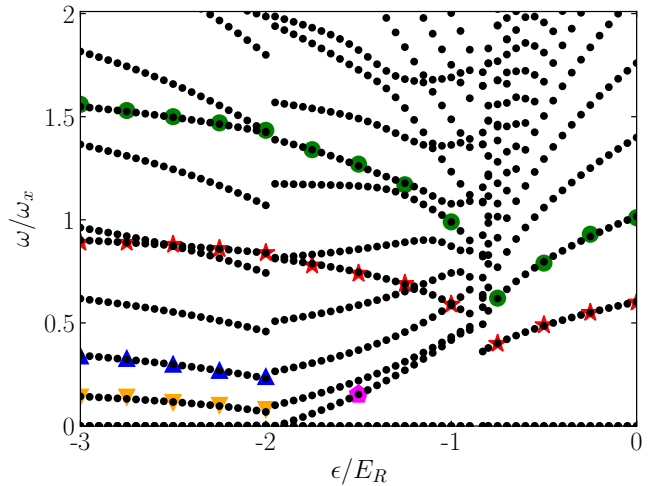


FIG. 4. Excitation spectrum of the SO coupled spin-1 BEC with  $c_0 = 59.44$ ,  $c_2 = 2.12$ ,  $k_R = 3$ , and  $\Omega = 3E_R$  as a function of quadratic Zeeman field strength  $\epsilon$ . The yellow up-triangle and blue down-triangle indicate the spin-dipole and spin-breathing modes, respectively. The yellow up-triangles and blue down-triangles indicate the spin-dipole and spin-breathing modes, respectively. At  $\epsilon_{c_1} \approx -2E_R$ , the ST phase transitions to the PW phase, and at  $\epsilon_{c_2} \approx -0.9E_R$  the PW phase transitions to the ZM phase. The discontinuous jumps in the dipole and the breathing modes across these transition points indicate the first-order nature of these transitions. In the PW phase, the roton excitation vanishing at the PW-ST phase boundary is marked by a magenta-coloured filled pentagon.

ST phase, the spin-dipole and the spin-breathing modes soften with an increase in Zeeman strength and have their minimum values at the ST-PW phase boundary,  $\epsilon_{c_1} \approx -2E_R$ ; the dipole and breathing modes, which decrease with increasing  $\epsilon$  across the ST and the PW phases, exhibit discontinuities across the first-order ST-PW phase transition point. However, the dipole and breathing modes jump discontinuously across the PW-ZM phase boundary at  $\epsilon_{c_2} \approx -0.9E_R$ , in contrast to the spectrum shown in Fig. 3, and then increase with increasing  $\epsilon$  across the ZM phase. This discontinuity in dipole and breathing modes indicates a first-order transition from the PW phase to the ZM phase. Another distinctive feature in this case: at  $\Omega_{c_2}$  in Fig. 3, dipole mode approaches zero, but there is a finite gap in Fig. 4 at  $\epsilon_{c_2}$ .

At lower values of  $\Omega$ , the phase transition directly from the ST to the ZM phase is observed as one varies  $\epsilon$  [14]. In Fig. 5, we plot the excitation spectrum of the BEC at a lower  $\Omega = E_R$  as a function  $\epsilon$ . Within the ZM phase, as the quadratic Zeeman strength is decreased, symmetric double roton modes decrease and vanish at the ZM-ST phase boundary,  $\epsilon_{c_1} \approx -0.12E_R$  [15, 26, 27]. The dipole, breathing, spin-dipole, and spin-breathing modes remain nearly constant in

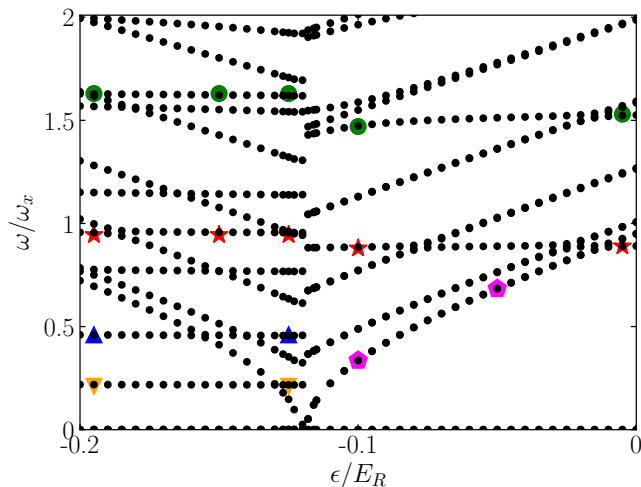


FIG. 5. Low-lying collective excitations of  $^{23}\text{Na}$  Raman-induced SO coupled spin-1 BEC with  $c_0 = 59.44$ ,  $c_1 = 2.12$ ,  $\Omega = E_R$ , and  $k_R = 3$  as a function of quadratic Zeeman field strength  $\epsilon$ . The density-dipole and density-breathing modes are marked by red asterisks and green-filled circles, respectively. The yellow up-triangles and blue down-triangles indicate the spin-dipole and spin-breathing modes, respectively. In the ZM phase, the softening of the lowest-lying double roton modes marked by magenta colored-filled pentagon indicates a phase transition from the ZM phase to the ST phase at  $\epsilon_{c_1} \approx -0.12 E_R$ . The dipole and breathing modes vary discontinuously across the first-order phase transition.

the ST phase, with the two density modes displaying discontinuities at (the first-order) transition point.

#### IV. COARSENING DYNAMICS IN A QUASI-2D SO-COUPLED BEC

In this section, we consider the coarsening dynamics [40, 41] in a homogenous quasi-2D SO-coupled spin-1 BEC initiated by a sudden quench of the coupling strength, resulting in the transition from the ZM phase to the PW phase. The ground state wave functions in the PW and ZM phases are of the form

$$\Phi(x, y) = \begin{bmatrix} \phi_1(x, y) \\ \phi_0(x, y) \\ \phi_{-1}(x, y) \end{bmatrix} = \sqrt{n} e^{ikx} \begin{pmatrix} \eta_1 e^{i\theta_1} \\ \eta_0 \\ \eta_{-1} e^{i\theta_3} \end{pmatrix}, \quad (10)$$

where  $n = N/A$  is the atom density (number of atoms per unit area), and  $k$  is the condensate's momentum, which is zero for the ZM and non-zero for the PW phase, and  $(\eta_{+1}, \eta_0, \eta_{-1})$  is a spinor with  $\sum_{j=\pm 1, 0} |\eta_j|^2 = 1$  [27]. The energy per particle in the PW (or ZM) phase, obtained by substituting  $\Phi$

in (10) in Eq. (1), is

$$\begin{aligned} \frac{E}{N} = & \frac{k^2}{2} + 2k(\eta_1^2 - \eta_3^2) + (\epsilon + 2)(\eta_1^2 + \eta_{-1}^2) + \frac{c_0 n}{2} \\ & + \sqrt{2}\Omega\eta_0(\eta_1 \cos \theta_1 + \eta_{-1} \cos \theta_3) + \frac{c_2 n}{2}(1 - 2\eta_{-1}^2)^2 \\ & + \frac{c_2 n \eta_0^2}{2} [4\eta_1 \eta_{-1} \cos(\theta_1 + \theta_3) + 4\eta_{-1}^2 - \eta_0^2], \end{aligned}$$

where length, time, and energy are in units  $1/k_R$ ,  $m/(\hbar k_R^2)$ , and  $\hbar^2 k_R^2/m$ , respectively. We calculate  $k$ ,  $\eta_{1,0,-1}$  and  $\theta_{1,3}$  across the PW and ZM phases by minimizing  $E/N$ . As noted for the harmonically confined quasi-1D BEC [see Fig. 1(a)],  $k$  decreases with an increase in  $\Omega$  and vanishes at the PW-ZM phase boundary. In this section, we consider  $c_0 n = 1$  and  $c_2 n = 0.1$  and quadratic Zeeman field strength ( $\epsilon$ ) = -1 which leads to  $\Omega_{c_2} \approx 2.75 E_R$ .

*Preparation of the initial state:* The PW phase breaks the  $\mathbb{Z}_2$  symmetry with non-zero longitudinal magnetization  $F_z$ , which serves as the order parameter for the phase. It is essential to prepare the initial state in the ZM phase by considering fluctuations to the mean-field ground state to initiate the formation of the symmetry-breaking domains after the coupling strength is quenched. Accordingly, we introduce noise to the ground-state solution using the truncated Wigner prescription [31]. To generate the noise, we consider the perturbation to the ground-state wavefunction of the ZM phase as  $\phi_j(x, y, t) = e^{-i\mu t} \left[ \sqrt{n_j} + (u_{\mathbf{q}}^j e^{i(\mathbf{q}\cdot\mathbf{r} - \omega t)} - v_{\mathbf{q}}^{j*} e^{-i(\mathbf{q}\cdot\mathbf{r} - \omega t)}) / \sqrt{A} \right]$  to write the BdG equations for a homogeneous quasi-2D SO-coupled BEC in the ZM phase, where  $\mathbf{q} = (q_x, q_y)$  is the quasi-momentum and  $u_{\mathbf{q}}$  and  $v_{\mathbf{q}}$  are the quasi-particle amplitudes. We numerically solve the homogenous BdG equations to obtain the quasiparticle amplitudes and the dispersion; a typical dispersion is shown in Fig. 6 for  $\Omega = 6$ . The noise to be added to the mean-field ground state is

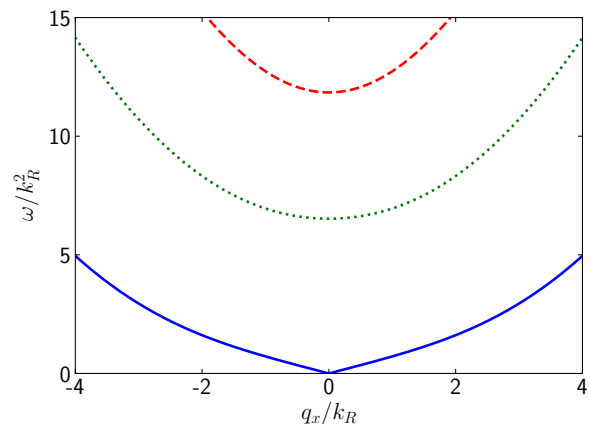


FIG. 6. The elementary excitation energies of a homogeneous quasi-2D SO-coupled spin-1 BEC with  $c_0 n = 1$ ,  $c_2 n = 0.1$ ,  $\Omega = 6$  and  $\epsilon = -1$  in the ZM phase as a function of quasi-momentum  $q_x$  for  $q_y$  fixed to zero.

$\delta_j(x, y) = \varepsilon \left( \sum_{\mathbf{q}} [\beta_{\mathbf{q}}^j v_{\mathbf{q}}^j e^{i\mathbf{q}\cdot\mathbf{r}} - \beta_{\mathbf{q}}^{j*} v_{\mathbf{q}}^{j*} e^{-i\mathbf{q}\cdot\mathbf{r}}] \right)$ , where  $\mathbf{q} = 0$  is excluded from the sum,  $\beta_{\mathbf{q}}^j$  are complex Gaussian random numbers with mean and variance equal to 0 and  $1/2$ , respectively [31], and  $\varepsilon$  is a small real number.

We consider a spatial 2D grid of  $1024 \times 1024$  spanning a spatial extent of  $800 \times 800$  with periodic boundary conditions to simulate the quench dynamics using the GPEs for the quasi-2D system (which can be obtained from Eqs. (4a) and (4b) by replacing  $\partial_x^2$  by  $\partial_x^2 + \partial_y^2$ ,  $V(x)$  by zero and  $k_R$  by 1. At  $t = 0$ , we suddenly quench Raman coupling to a value corresponding to which the ground-state phase is the PW phase. After the quench, the system develops longitudinal magnetization ( $F_z$ ). The evolution of  $\langle F_z^2 \rangle$  post-quench is illustrated in Fig. 7, where  $\langle \dots \rangle$  denotes the ensemble average with different members of the ensemble obtained by the quench dynamics corresponding to different initial noises  $\delta_j(x, y)$  added to the ground-state solution at  $t = 0$ . We consider an ensemble

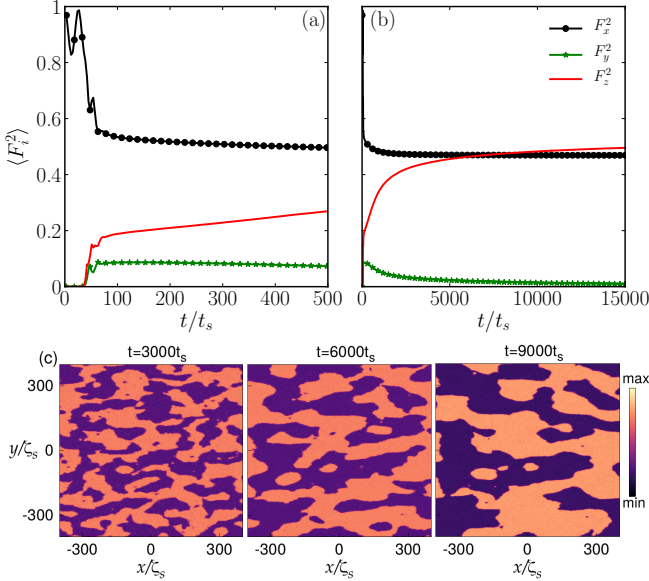


FIG. 7. (a) and (b): Time evolution of  $\langle F_z^2 \rangle$  following a quench from the ZM phase with  $\Omega = 6$  to the PW phase with  $\Omega = 2$ . In the ZM phase,  $F_x = -1$ , while  $F_z = 0$ . (c) Longitudinal magnetization density  $F_z(x, y)$  at different times for a particular ensemble member. The domain sizes are progressively increasing with time.

average over 30 simulations. Initially, at  $t = 0$ , both  $\langle F_y^2 \rangle$  and  $\langle F_z^2 \rangle$  are zero, while  $\langle F_x^2 \rangle$  is equal to 1 [see Fig. 7(a)]. Between  $t \approx 20t_s$  to  $t \approx 60t_s$ ,  $\langle F_z^2 \rangle$  grows exponentially; as more time elapses, the magnetization starts to saturate steadily [see Fig. 7(b)], and the domain begins to coarsen; domains of the  $F_z(x, y)$  at different times for a single noise realization are shown in Fig. 7(c). As the domains coarsen, the coarsening dynamics become universal and independent of the microscopic details. By using the translational invariance of the system and isotropy of the 2D space, these domains are de-

scribed by the order parameter autocorrelation function [34]

$$G(r, t) = \left\langle \frac{1}{A} \left\langle \int d\mathbf{r}' F_z(\mathbf{r}', t) F_z(\mathbf{r}' + \mathbf{r}, t) \right\rangle_{\text{ang}} \right\rangle, \\ = \left\langle \sum_{\mathbf{k}} |\tilde{F}_z(\mathbf{k}, t)|^2 J_0(kr) \right\rangle, \quad (11)$$

where  $\tilde{F}_z(\mathbf{k}, t)$  denotes the discrete Fourier transform of  $F_z(\mathbf{r}, t)$ ,  $J_0(kr)$  is the zeroth order Bessel function of first kind,  $\langle \dots \rangle_{\text{ang}}$  denotes the angular average. The correlation

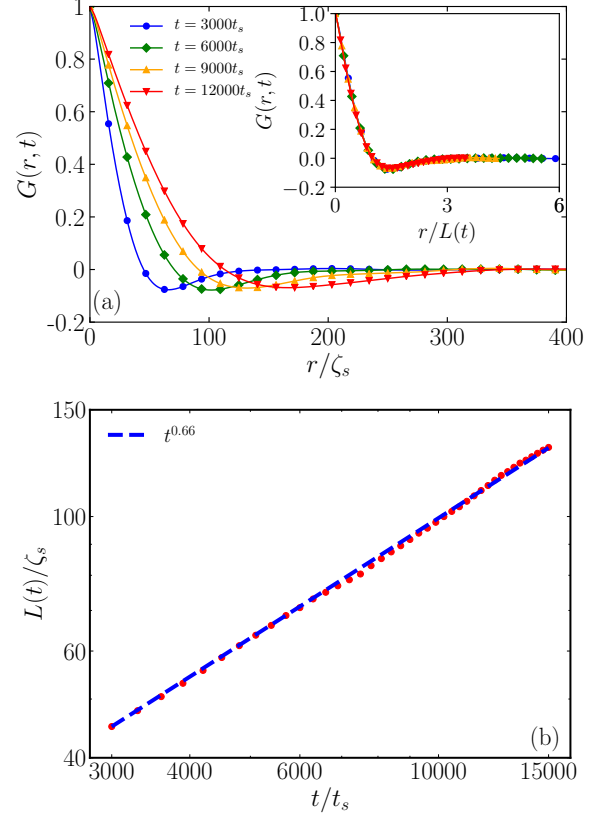


FIG. 8. (a) Correlation function  $G(r, t)$  at different times; inset: the correlation functions  $G(r/L(t), t)$  with the spatial coordinates rescaled by  $L(t)$  collapsing onto a single function demonstrating the universal coarsening behavior. (b) the characteristic length  $L(t)$  as a function of  $t$  (red dots) and the best-fit  $L(t) \sim t^{0.66}$  (dashed-blue line).

functions at different times are shown in Fig. 8, and as time elapses during the coarsening dynamics, the correlations extend over a broader spatial domain. We define the average domain size  $L(t)$  as the first zero of the correlation function  $G(r, t)$ . When one measures the spatial coordinates in the units of  $L(t)$ , the correlation functions at different times fall on a single curve  $f(r) = G(r/L(t), t)$ . This demonstrates the universal coarsening behavior (see the inset of Fig. 8). The characteristic length  $L(t)$  grows as a power law with time, as shown in Fig. 8(b). We find that for a range of  $\Omega$  values  $L(t) = (t/t_0)^\beta L_0$  with a dynamic critical exponent

$\beta = 0.66$ , where  $L_0$  is the characteristic length scale at an arbitrary reference time  $t_0$ . We find that the quenching from the ZM to the PW phase by a sudden decrease of quadratic Zeeman field  $\epsilon$  below  $\epsilon_{c2}$  demonstrates the same power-law scaling with  $\beta = 0.66$  (results not shown here). These results indicate that the late-time post-quench dynamics from the PW to the ZM phase in an SO-coupled BEC belongs to a binary fluid universality class in the inertial hydrodynamic regime [30, 33, 38, 40, 64].

## V. SUMMARY AND CONCLUSIONS

In the first part of this study, we examine the collective excitations of a harmonically trapped quasi-1D SO-coupled spin-1 BEC. We analyze the dependence of these excitations on two experimentally controllable parameters: the Raman coupling and the Zeeman field strengths. By examining the behavior of excitation modes, we identify key signatures of phase transitions between different quantum phases. We calculate dipole and breathing modes for density and spin channels by applying appropriate perturbations to the system. The spin-dipole and spin-breathing modes soften near the ST-PW phase boundary, whereas the density-dipole and density-breathing modes soften near the PW-ZM phase. At lower values of Raman coupling strength, the system can show a direct transition from the ZM to the ST phase with a variation in the quadratic Zeeman field. In this case, as the system approaches the transition to the ST phase, we observe the softening of a double symmetric roton mode, indicating the system's tendency towards crystallization. Furthermore, we confirm the order of

the phase transitions by examining momentum and the spin expectation per particle of the condensate across the three phases, which agree with the behavior of the collective excitations, especially the two density modes, across the transition points.

In the second part of this study, we focus on the universal coarsening dynamics of a homogeneous quasi-2D SO-coupled spin-1 BEC by quenching Raman coupling (or quadratic Zeeman field strength) from the ZM to the PW phase. We demonstrate that the correlation function of the order parameter displays dynamic scaling during the late-time dynamics, allowing us to determine the dynamic critical exponent. We show the formation of magnetic domains and the universal behavior of the correlation function of order parameters as it scales by a characteristic length  $L(t)$ . This characteristic length increases with time following a power law  $L(t) \sim t^{0.66}$ . This finding is consistent with the inertial hydrodynamics domain growth law of binary fluids.

## Acknowledgements

We acknowledge the National Supercomputing Mission (NSM) for providing computing resources of 'PARAM SM-RITI' at NABI, Mohali, and 'PARAM Ananta' at IIT Gandhinagar, which is implemented by C-DAC and supported by the Ministry of Electronics and Information Technology (MeitY) and Department of Science and Technology (DST), Government of India. SG acknowledges support from the Science and Engineering Research Board, Department of Science and Technology, Government of India through Project No. CRG/2021/002597.

- 
- [1] Y.-J. Lin, R. L. Compton, K. Jimenez-Garcia, W. D. Phillips, J. V. Porto, and I. B. Spielman, *Nature Physics* **7**, 531 (2011).
  - [2] N. Goldman, G. Juzeliūnas, P. Öhberg, and I. B. Spielman, *Reports on Progress in Physics* **77**, 126401 (2014).
  - [3] V. Galitski and I. B. Spielman, *Nature* **494**, 49 (2013).
  - [4] Y.-J. Lin, K. Jiménez-García, and I. B. Spielman, *Nature (London)* **471**, 83 (2011).
  - [5] D. Campbell, R. Price, A. Putra, A. Valdés-Curiel, D. Trypogergos, and I. Spielman, *Nat. Commun.* **7**, 1 (2016).
  - [6] X. Luo, L. Wu, J. Chen, Q. Guan, K. Gao, Z.-F. Xu, L. You, and R. Wang, *Sci. Rep.* **6**, 1 (2016).
  - [7] H. Zhai, *Rep. Prog. Phys.* **78**, 026001 (2015).
  - [8] T.-L. Ho and S. Zhang, *Phys. Rev. Lett.* **107**, 150403 (2011).
  - [9] Y. Li, L. P. Pitaevskii, and S. Stringari, *Phys. Rev. Lett.* **108**, 225301 (2012).
  - [10] G. I. Martone and S. Stringari, *SciPost Phys.* **11**, 092 (2021).
  - [11] J.-R. Li, J. Lee, W. Huang, S. Burchesky, B. Shteynas, F. Ç. Top, A. O. Jamison, and W. Ketterle, *Nature* **543**, 91 (2017).
  - [12] A. Putra, F. Salces-Cárcoba, Y. Yue, S. Sugawa, and I. B. Spielman, *Phys. Rev. Lett.* **124**, 053605 (2020).
  - [13] K. T. Geier, G. I. Martone, P. Hauke, W. Ketterle, and S. Stringari, *Phys. Rev. Lett.* **130**, 156001 (2023).
  - [14] G. I. Martone, F. V. Pepe, P. Facchi, S. Pascazio, and S. Stringari, *Phys. Rev. Lett.* **117**, 125301 (2016).
  - [15] Z.-Q. Yu, *Phys. Rev. A* **93**, 033648 (2016).
  - [16] C. J. Pethick and H. Smith, *Bose-Einstein Condensation in Dilute Gases* (Cambridge University Press, 2008).
  - [17] L. Pitaevskii and S. Stringari, *Bose-Einstein condensation and superfluidity*, Vol. 164 (Oxford University Press, 2016).
  - [18] G. I. Martone, Y. Li, L. P. Pitaevskii, and S. Stringari, *Phys. Rev. A* **86**, 063621 (2012).
  - [19] Y. Li, G. I. Martone, L. P. Pitaevskii, and S. Stringari, *Phys. Rev. Lett.* **110**, 235302 (2013).
  - [20] M. A. Khamehchi, Y. Zhang, C. Hamner, T. Busch, and P. Engels, *Phys. Rev. A* **90**, 063624 (2014).
  - [21] S.-C. Ji, L. Zhang, X.-T. Xu, Z. Wu, Y. Deng, S. Chen, and J.-W. Pan, *Phys. Rev. Lett.* **114**, 105301 (2015).
  - [22] L. Chen, H. Pu, Z.-Q. Yu, and Y. Zhang, *Phys. Rev. A* **95**, 033616 (2017).
  - [23] K. T. Geier, G. I. Martone, P. Hauke, and S. Stringari, *Phys. Rev. Lett.* **127**, 115301 (2021).
  - [24] Rajat, Ritu, A. Roy, and S. Gautam, *Phys. Rev. A* **109**, 033319 (2024).
  - [25] W. Zheng, Z.-Q. Yu, X. Cui, and H. Zhai, *Journal of Physics B: Atomic, Molecular and Optical Physics* **46**, 134007 (2013).
  - [26] K. Sun, C. Qu, Y. Xu, Y. Zhang, and C. Zhang, *Phys. Rev. A* **93**, 023615 (2016).



- [27] Y. Chen, H. Lyu, Y. Xu, and Y. Zhang, *New Journal of Physics* **24**, 073041 (2022).
- [28] Rajat, A. Roy, and S. Gautam, *Phys. Rev. A* **106**, 013304 (2022).
- [29] A. Bourges and P. B. Blakie, *Phys. Rev. A* **95**, 023616 (2017).
- [30] S. Huh, K. Mukherjee, K. Kwon, J. Seo, J. Hur, S. I. Mistakidis, H. Sadeghpour, and J.-y. Choi, *Nature Physics* **20**, 402 (2024).
- [31] P. B. Blakie, A. S. Bradley, M. J. Davis, R. J. Ballagh, and C. W. Gardiner, *Advances in Physics* **57**, 363 (2008).
- [32] A. Bray, *Adv. Phys.* **43**, 357 (1994).
- [33] J. Hofmann, S. S. Natu, and S. Das Sarma, *Phys. Rev. Lett.* **113**, 095702 (2014).
- [34] K. Fujimoto, K. Haneda, K. Kudo, and Y. Kawaguchi, *Phys. Rev. A* **101**, 023608 (2020).
- [35] V. P. Singh, L. Amico, and L. Mathey, *Phys. Rev. Res.* **5**, 043042 (2023).
- [36] A. Lamacraft, *Phys. Rev. Lett.* **98**, 160404 (2007); M. Uhlmann, R. Schützhold, and U. R. Fischer, *Phys. Rev. Lett.* **99**, 120407 (2007); *Phys. Rev. D* **81**, 025017 (2010); M. Uhlmann, R. Schützhold, and U. R. Fischer, *New Journal of Physics* **12**, 095020 (2010).
- [37] S. Mukerjee, C. Xu, and J. E. Moore, *Phys. Rev. B* **76**, 104519 (2007).
- [38] K. Kudo and Y. Kawaguchi, *Phys. Rev. A* **88**, 013630 (2013).
- [39] K. Kudo and Y. Kawaguchi, *Phys. Rev. A* **91**, 053609 (2015).
- [40] L. A. Williamson and P. B. Blakie, *Phys. Rev. Lett.* **116**, 025301 (2016).
- [41] L. A. Williamson and P. B. Blakie, *Phys. Rev. A* **94**, 023608 (2016).
- [42] L. A. Williamson and P. B. Blakie, *Phys. Rev. Lett.* **119**, 255301 (2017).
- [43] L. M. Symes and P. B. Blakie, *Phys. Rev. A* **96**, 013602 (2017).
- [44] L. M. Symes, D. Baillie, and P. B. Blakie, *Phys. Rev. A* **98**, 063618 (2018).
- [45] K. Fujimoto, R. Hamazaki, and M. Ueda, *Phys. Rev. Lett.* **120**, 073002 (2018).
- [46] C.-M. Schmied, T. Gasenzer, and P. B. Blakie, *Phys. Rev. A* **100**, 033603 (2019).
- [47] C.-M. Schmied, M. Prüfer, M. K. Oberthaler, and T. Gasenzer, *Phys. Rev. A* **99**, 033611 (2019).
- [48] K. Fujimoto, R. Hamazaki, and M. Ueda, *Phys. Rev. Lett.* **122**, 173001 (2019).
- [49] J. Pietraszewicz, A. Seweryn, and E. Witkowska, *Scientific Reports* **11**, 9296 (2021).
- [50] M. Prüfer, P. Kunkel, H. Strobel, S. Lannig, D. Linnemann, C.-M. Schmied, J. Berges, T. Gasenzer, and M. K. Oberthaler, *Nature* **563**, 217 (2018).
- [51] I. Siovitz, S. Lannig, Y. Deller, H. Strobel, M. K. Oberthaler, and T. Gasenzer, *Phys. Rev. Lett.* **131**, 183402 (2023).
- [52] S. Erne, R. Bücker, T. Gasenzer, J. Berges, and J. Schmiedmayer, *Nature* **563**, 225 (2018).
- [53] J. A. Glidden, C. Eigen, L. H. Dogra, T. A. Hilker, R. P. Smith, and Z. Hadzibabic, *Nature Physics* **17**, 457 (2021).
- [54] A. D. García-Orozco, L. Madeira, M. A. Moreno-Armijos, A. R. Fritsch, P. E. S. Tavares, P. C. M. Castilho, A. Cidrim, G. Roati, and V. S. Bagnato, *Phys. Rev. A* **106**, 023314 (2022).
- [55] Z. Lan and P. Öhberg, *Phys. Rev. A* **89**, 023630 (2014).
- [56] L. Salasnich, A. Parola, and L. Reatto, *Phys. Rev. A* **65**, 043614 (2002).
- [57] P. Kaur, A. Roy, and S. Gautam, *Comput. Phys. Commun.* **259**, 107671 (2021); P. Banger, P. Kaur, A. Roy, and S. Gautam, *Comput. Phys. Commun.* **279**, 108442 (2022); P. Banger, P. Kaur, and S. Gautam, *Int. J. Mod. Phys. C* **33**, 2250046 (2022).
- [58] A. Roy, S. Pal, S. Gautam, D. Angom, and P. Muruganandam, *Comput. Phys. Commun.* **256**, 107288 (2020).
- [59] <https://www.netlib.org/lapack/>.
- [60] R. B. Lehoucq, D. C. Sorensen, and C. Yang, *ARPACK Users' Guide* (Society for Industrial and Applied Mathematics, 1998) <https://epubs.siam.org/doi/pdf/10.1137/1.9780898719628>.
- [61] M.-O. Mewes, M. R. Andrews, N. J. van Druten, D. M. Kurn, D. S. Durfee, C. G. Townsend, and W. Ketterle, *Phys. Rev. Lett.* **77**, 988 (1996).
- [62] T. Bienaimé, E. Fava, G. Colzi, C. Mordini, S. Serafini, C. Qu, S. Stringari, G. Lamporesi, and G. Ferrari, *Phys. Rev. A* **94**, 063652 (2016).
- [63] S. Knoop, T. Schuster, R. Scelle, A. Trautmann, J. Appmeier, M. K. Oberthaler, E. Tiesinga, and E. Tiemann, *Phys. Rev. A* **83**, 042704 (2011).
- [64] H. Furukawa, *Phys. Rev. A* **31**, 1103 (1985).